Real-space renormalization-group treatment of the Maier-Saupe-Zwanzig model for biaxial nematic structures

Cícero T. G. dos Santos [1,2] André P. Vieira [3] Silvio R. Salinas [3] and Roberto F. S. Andrade [1,4]

[1] *Instituto de Física, Universidade Federal da Bahia, 40170-115 Salvador, Brazil*

[2] *Instituto Federal de Educação, Ciência e Tecnologia do Sertão Pernambucano, 56302-100 Petrolina, Brazil*

[3] *Universidade de Sao Paulo, Instituto de Fisica, Rua do Matao, 1371, 05508-090 Sao Paulo, SP, Brazil*

[4] *Centre for Data and Knowledge Integration for Health (CIDACS), Instituto Gonçalo Moniz, Fundação Oswaldo Cruz, 41745-715 Salvador, Brazil*

(Received 6 October 2020; revised 17 November 2020; accepted 11 February 2021; published 10 March 2021)

The Maier-Saupe-Zwanzig model for the nematic phase transitions in liquid crystals is investigated in a diamond hierarchical lattice. The model takes into account a parameter to describe the biaxiality of the microscopic units. Also, a suitably chosen external field is added to the Hamiltonian to allow the determination of critical parameters associated with the nematic phase transitions. Using the transfer-matrix technique, the free energy and its derivatives are obtained in terms of recursion relations between successive generations of the hierarchical lattice. In addition, a real-space renormalization-group approach is developed to obtain the critical parameters of the same model system. Results of both methods are in excellent agreement. There are indications of two continuous phase transitions. One of them corresponds to a uniaxial-isotropic transition, in the class of universality of the three-state Potts model on the diamond hierarchical lattice. The transition between the biaxial and the uniaxial phases is in the universality class of the Ising model on the same lattice.

DOI: 10.1103/PhysRevE.103.032111

I. INTRODUCTION

Liquid crystals are intermediate phases of matter with rich macroscopic patterns associated with orientational order [1]. Nematic liquid crystals are perhaps the best known and investigated class of these systems. From a microscopic point of view, these nematic systems consist of anisotropic molecular or micellar structures, which we call nematogens, and which are associated with microscopic directors. This general term refers to the microscopic components of a large class of systems with quite different properties, including thermotropic and lyotropic (or colloidal) liquid crystals. In a simple uniaxial nematic phase, on the average these microscopic directors are aligned along a preferred direction. As we increase the temperature, there may be a usually weak and discontinuous transition to a disordered structure, which is perhaps the best studied phase transition phenomenon in liquid crystalline systems [2]. A macroscopic rotational symmetry breaking around a preferred nematic direction can lead to a nematic phase with three independent directions, which is known as the biaxial nematic phase [3]. In general, cylindrical or ellipsoidal nematogens give rise to uniaxial phases only, but biaxial nematic structures cannot be ruled out. These biaxial nematic structures have been predicted theoretically by Freiser a long time ago [4], have been initially found in micellar systems [5], and seem nowadays to have been characterized in some anisotropic board-shaped nematogens [6], more specifically in those with a significant degree of size dispersivity [7]. Following a possible but still somewhat controversial experimental identification of thermotropic biaxial nematic liquid crystals [8–12], a large number of experimental, computational, and theoretical investigations have found a new stimulus [13].

The transition from a uniaxial nematic to an isotropic liquid crystalline phase can be accounted for by the mean-field Maier-Saupe theory [14], which plays a prominent role among the theoretical descriptions of liquid crystalline transitions. This theory also leads to the well-known form of the Landau–de Gennes expansion of the free energy in terms of a tensor order parameter, with the cubic term that guarantees the first-order character of the transition between uniaxial nematic and disordered phases [1]. On the basis of this approach, we can devise a bona fide lattice statistical model, with quadrupolar variables on the lattice sites, and with the energy restricted to pair interactions. A fully connected version of this model, which we call the Maier-Saupe (MS) model, and which is analogous of the Curie-Weiss model of magnetism, leads to the known results of the nematic mean-field theory. Also, according to the work of Freiser, it is possible to introduce biaxial elements in the Maier-Saupe theory, which lead to stable biaxial structures at low temperatures, and to a second-order biaxial-uniaxial phase transition.

The Maier-Saupe approach can be combined with an assumption of discrete orientations of the microscopic directors associated with the nematogens. This approximation was originally proposed by Zwanzig [15] in the context of a work with the hard cylinder model of Onsager for the nematic transition, and has been later adopted by a number of authors [16–23]. Although it may not be adequate to account for the properties of systems with hard boardlike particles [24–26], it has been used to obtain a number of equilibrium features of

nematic systems. At the mean-field level of treatment, it has been shown to compare quite well with analogous treatments [27–31]. In this work, we then consider a three-state lattice model system, which we call MSZ, and whose fully connected version can be easily analyzed by standard statistical mechanics techniques [23,28,29]. We can as well introduce some modifications in the original MSZ model with a view at explaining the onset of biaxial phases. We then consider additional microscopic possibilities, and define a six-state model, which we call MSZ6, and which can be shown to be equivalent to a lattice statistical model originally proposed by Boccara, Medjani, and de Sèze [32], to reproduce the well-known sequence of isotropic, uniaxial, and biaxial nematic phases as a function of decreasing temperature and the onset of a Landau multicritical point [4]. More recently, we have investigated the connections of these statistical formulations with some proposals of a quite general two-tensor formalism, at the mean-field level, which is able to describe the classical isotropic-uniaxial-biaxial sequence of phases in the nematic systems as well as some novel features of the phase diagrams [33]. The MSZ6 model that we work with corresponds to the two-tensor formalism with the choice of interaction parameters according to a very much used geometric mean approximation. Except for a calculation on the Bethe lattice [34], the investigations of the MSZ and MSZ6 models have been restricted to fully connected systems, at the mean-field level, without any attempt at considering the role of statistical fluctuations.

In this work we present a real-space renormalization-group (RSRG) analysis of the MSZ6 model. We work on hierarchical lattices [35–37], for which RSRG results are exact and correspond to those obtained from the Migdal-Kadanoff bond-moving RSRG approximation for the analogous models on a Bravais lattice. Although these results may be quantitatively different from the findings for the corresponding model systems on translational invariant lattices, especially when it comes to critical exponents and universality [38–40], these calculations on hierarchical lattices can be helpful to reveal certain features of the phase diagrams that may be mere artifacts of the mean-field treatments. We present a renormalization-group calculation to deal with the biaxial-uniaxial transition. Although the use of a hierarchical lattice does not capture the discontinuous nature of the uniaxial-isotropic transition, as it is also found in a similar real-space treatment for the Lebwohl-Lasher model [41], we have been able to reproduce all the remaining aspects of the mean-field phase diagram, including the presence of two uniaxial phases and of a Landau multicritical point.

In Sec. II, we define the MSZ6 model system. For a matter of convenience, we include two fictitious external fields which are meant to enable a quantitative description of the average molecular orientation in different phases. Also, we describe the construction of the diamond hierarchical lattice (DHL) and discuss its main properties. In Sec. III, we describe the two real-space renormalization-group methods that are used in this work. We obtain analytic expressions for the maps associated with the transfer-matrix approach, and discuss the assumptions to implement the RSRG formalism. Due to the complexity of the model, large expressions are moved to the Supplemental Material [42]. Results obtained by both methods are presented in Sec. IV. We point out the excellent agreement between the corresponding results. In the final section, we present some concluding remarks, with emphasis on the more interesting results. We point out that there are indications of two continuous phase transitions. One of them corresponds to a uniaxial-isotropic transition, in the class of universality of the three-state Potts model on the diamond hierarchical lattice. The transition between the biaxial and the uniaxial phases is in the universality class of the Ising model on the same lattice.

II. DEFINITION OF THE MODEL SYSTEMS

A. Elementary MSZ model for biaxial liquid crystals

The general form of the nearest-neighbor MSZ model on a crystal lattice is given by the Hamiltonian

$$\mathcal{H}_0 = -\epsilon \sum_{(i,j)} \sum_{\alpha,\beta=x,y,z} \Omega_i^{\alpha\beta} \Omega_j^{\alpha\beta}, \tag{1}$$

where ϵ is a positive parameter, the first sum is performed over nearest-neighbor pairs (i, j) of nematogens on sites i and j, and $\Omega_i^{\alpha\beta}$ are the components of a second rank, traceless tensor associated with a nematogen at the ith site in the laboratory reference system. If one decides to restrict the formalism by directly working in the basis where Ω is diagonal, the sums over the tensor indices α and β in Eq. (1) can be expressed in terms of a scalar product between vectors formed by the diagonal elements of the tensor. For the sake of presenting the general framework, throughout this work we will continue to explicitly indicate the tensor sums. In the MSZ6 model, $\mathbf{\Omega}$ has the generic form

$$\mathbf{\Omega} = \begin{pmatrix} 2 & 0 & 0 \\ 0 & -1+\Delta & 0 \\ 0 & 0 & -1-\Delta \end{pmatrix}. \tag{2}$$

In this formulation, each nematogen is represented by a general parallelepiped with three different edge lengths that can only be aligned along six directions determined by the Cartesian directions of the laboratory. Therefore, the quadrupole tensor $\mathbf{\Omega}$ can assume only six states, given by Eq. (2) and respective permutations of the main diagonal elements. Parameter Δ is associated with the molecular biaxiality. If $\Delta < 1$, the rodlike nematogen geometry gives rise to a prolate uniaxial phase, while the $\Delta > 1$ disklike shapes lead to an oblate uniaxial phase.

If $\Delta = 0$ or 3, the model is intrinsically uniaxial and equivalent to a three-state Potts model. If $0 < \Delta < 3$, the model turns out to be properly able to describe a biaxial phase. Note that the energy spectrum of $\mathcal{H}_0$ for $\Delta > 3$ can be mapped onto that for $1 < \Delta < 3$ [28], so that is sufficient to restrict the study to the choice $0 \leqslant \Delta \leqslant 3$.

The nematogens of a usual liquid crystal are not linearly coupled to external fields, as it is the case in ferromagnetic or ferroelectric systems. In fact, their response to an imposed field is comparably weaker, and the actual nature of these interactions is rather involved. Nevertheless, in the spirit of the statistical mechanics approach to models with discrete energy levels, and irrespective of whether an actual physical meaning can be assigned to it, we find it useful to include in

the Hamiltonian the contribution of a generic external field that can be written as

$$\mathcal{H}_f = -\sum_i \sum_{\alpha,\beta=x,y,z} \left[h_x \Omega_i^{\alpha\beta}\delta(\alpha,x)\delta(\beta,x) + h_y \Omega_i^{\alpha\beta}\delta(\alpha,y)\delta(\beta,y)\right]. \quad (3)$$

For the sake of clarity, we have arbitrarily chosen x and y as the directions for the alignment of the nematogens that characterize the two order parameters. We remind that any of other five possible choices give rise to equivalent results. In Eq. (3), $\delta(\cdot,\cdot)$ indicates the Kronecker delta of the arguments and is used to select the components of $\mathbf{\Omega}$ in which the external fields will act, in a similar way as in the Potts model [43]. Therefore, the total Hamiltonian of the system is given by $\mathcal{H} = \mathcal{H}_0 + \mathcal{H}_f$.

To quantify the degree of molecular ordering in a liquid crystal under given temperature conditions, one defines a tensor order parameter $\mathbf{Q} \equiv \langle \mathbf{\Omega} \rangle$ representing the thermal average of the distribution of molecular orientations. We thus have $Q^{\mu\nu} = \langle \Omega^{\mu\nu} \rangle$, and introducing $s_x = \sum_i \Omega_i^{xx}/N$ and $s_y = \sum_i \Omega_i^{yy}/N$, where N represents the number of nematogens, we can define m_x and m_y as

$$m_x \equiv \langle s_x \rangle = \frac{1}{Z}\sum_{\{\mathbf{\Omega}\}} s_x e^{-\mathcal{H}/k_B T} \quad (4)$$

and

$$m_y \equiv \langle s_y \rangle = \frac{1}{Z}\sum_{\{\mathbf{\Omega}\}} s_y e^{-\mathcal{H}/k_B T}, \quad (5)$$

in which k_B is Boltzmann's constant, T is the temperature, Z is the partition function

$$Z = \sum_{\{\mathbf{\Omega}\}} e^{-\mathcal{H}/k_B T}, \quad (6)$$

and the sums run over all sets of states $\{\mathbf{\Omega}\}$ of all nematogens in the system. Finally, m_x and m_y can be connected to the scalar order parameters S and η, respectively the uniaxial and biaxial order parameters, by considering $\mathbf{Q}$ in its diagonal form

$$\mathbf{Q} = \begin{pmatrix} S & 0 & 0 \\ 0 & -\frac{1}{2}(S-\eta) & 0 \\ 0 & 0 & -\frac{1}{2}(S+\eta) \end{pmatrix} \quad (7)$$

for $\Delta \leqslant 1$, and

$$\mathbf{Q} = \begin{pmatrix} -\frac{1}{2}(S-\eta) & 0 & 0 \\ 0 & -\frac{1}{2}(S+\eta) & 0 \\ 0 & 0 & S \end{pmatrix} \quad (8)$$

for $\Delta > 1$. This choice leads to $S > 0$ in a rodlike uniaxial phase, which is expected for $\Delta < 1$, and $S < 0$ in a disklike uniaxial phase, which is expected for $\Delta > 1$.

From Eqs. (4) and (5) and the preceding discussion, we can also write

$$\mathbf{Q} = \begin{pmatrix} m_x & 0 & 0 \\ 0 & m_y & 0 \\ 0 & 0 & -m_x - m_y \end{pmatrix}, \quad (9)$$

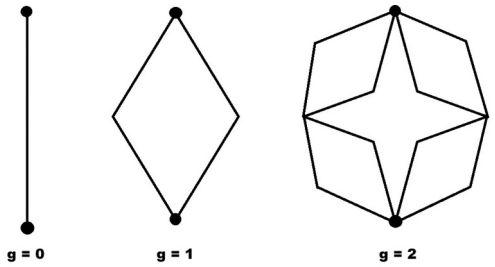

FIG. 1. First two steps of construction of the $p = b = 2$ DHL. Generation $g = 1$ defines its generator.

so that, comparing with Eqs. (7) and (8), we obtain

$$\begin{cases} S = & m_x, \\ \eta = & m_x + 2m_y \end{cases} \quad (10)$$

for $\Delta \leqslant 1$, and

$$\begin{cases} S = & -m_x - m_y, \\ \eta = & m_x - m_y \end{cases} \quad (11)$$

for $\Delta > 1$.

B. Diamond hierarchical lattice

Hierarchical lattices [36] are built recursively by replacing each link between two sites in a given generation by a pattern called the *generator*. The DHL is built by starting from two root sites connected by a single link. In the first generation, this single link is replaced by p parallel branches, each one of them connecting the root sites via b internal links and $b-1$ internal sites. In the subsequent generations, each link is replaced by the same generator. The fractal dimension for this family of lattices is given by $d_f = 1 + (\ln p)/(\ln b)$. The numbers of sites and links at the gth generation are, respectively, given by $N_g = (b-1)p[(bp)^g - 1]/(bp-1)$ and $L_g = (bp)^g$. In this work, for the sake of simplicity we consider only the most used case $p = b = 2$, i.e., $d_f = 2$, but we checked that the results are qualitatively independent of the fractal dimension as long as it is greater than or equal to 2. The lattice with fractal dimension $d_f = 2$ is illustrated in Fig. 1. The distribution of connections at each site is highly inhomogeneous, as it becomes clear for larger generations.

Results for physical models on hierarchical lattices have a tendency to qualitatively agree with those for actual regular Bravais lattices, albeit the quantitative comparison may present considerable discrepancies [44]. With this proviso, results for such geometrical constructs may be regarded as valuable approximations for actual systems. Indeed, it is well known that the Migdal-Kadanoff real-space renormalization-group approach to the two-dimensional Ising model is equivalent to the same model in the $b = p = 2$ DHL investigated in this work.

III. DHL CALCULATIONS

As it can be seen from the recursive construction mechanism, DHLs have a scale invariance property. Thus, models on these lattices are suitable to be analyzed by methods that explicitly take into account these intrinsic properties. Both

approaches implemented in this work are based on scale invariance, and have been extensively used in previous studies for much simpler interaction models. In the sequence we present the key steps used for the derivation of the expressions, leading to the results discussed in the next section.

A. Transfer matrices for the MSZ6 model on DHLs

A transfer-matrix (TM) formulation for hierarchical lattices such as the DHL has been used to obtain the thermodynamic functions of several statistical models [45–47]. The general idea is to obtain the free energy in the gth generation from the one in the $(g-1)$th generation. This can be achieved due to the lattice geometrical self-similarity, which warrants that the matrix elements in the gth generation can be written as a function of those in the $(g-1)$th generation by a recurrence map. As the matrix elements in the different generations preserve the same structure, it happens that the eigenvalues of two successive generations are expressed in the same way as a function of the corresponding matrix elements. Therefore, for some models, it is even possible to write a direct recursive map for the eigenvalues Λ_g in the gth generation in terms of those in generation $g-1$. As a consequence, the free energy, written in terms of the largest eigenvalue of the TM, can also be obtained as a recurrence relation between successive generations.

We then write

$$f_g = -\frac{k_B T}{N_g}\ln(\Lambda_g), \tag{12}$$

where Λ_g is the largest eigenvalues of the TM in the gth generation and N_g is the corresponding number of sites. Let us start at $g=0$, when the lattice consists of two root sites connected by one single interaction term. For the purpose of simplifying the calculation, it is possible to assume that root sites are not subject to the external fields, which will only be included in the internal sites appearing in the successive generations. In such case, the 6×6 TM, $\bar{M}_0$, for the MSZ6 model is written as

$$\bar{M}_0 = \begin{pmatrix} a_0 & b_0 & c_0 & d_0 & d_0 & e_0 \\ b_0 & a_0 & d_0 & e_0 & c_0 & d_0 \\ c_0 & d_0 & a_0 & b_0 & e_0 & d_0 \\ d_0 & e_0 & b_0 & a_0 & d_0 & c_0 \\ d_0 & c_0 & e_0 & d_0 & a_0 & b_0 \\ e_0 & d_0 & d_0 & c_0 & b_0 & a_0 \end{pmatrix}, \tag{13}$$

where $a_0=\exp[(6+2\Delta^2)/k_BT]$, $b_0=\exp[(6-2\Delta^2)/k_BT]$, $c_0=\exp[(-3+6\Delta+\Delta^2)/k_BT]$, $d_0=\exp[(-3-\Delta^2)/k_BT]$, $e_0=\exp[(-3-6\Delta+\Delta^2)/k_BT]$. In the gth generation, the corresponding TM, $\bar{M}_g$, has exactly the same distribution of matrix elements $a_g,\ldots,e_g$, which respectively replace $a_0,\ldots,e_0$ in Eq. (13). Therefore, for any g, the matrix elements of $\bar{M}_g$ can be expressed in a recursive way in terms of those of $\bar{M}_{g-1}$. For the sake of simplicity, we may consider the case $g=1$. As illustrated in detail elsewhere [45], the field free $\bar{M}_1$ TM can be obtained with the help of $\bar{B}_1$, a 6×36 TM with elements

$$(\bar{B}_1)_{i,jk} = (\bar{B}_1)_{i,\kappa} = (M_0)_{i,j}(M_0)_{i,k}, \tag{14}$$

where $i,j,k=1,\ldots,6$ and $\kappa = 6(j-1)+k$. $\bar{B}_1$, which accounts for all interactions between one root site and the two newly introduced internal sites at $g=1$, is characterized by the following arrange of its 15 matrix elements

$$\bar{B}_1 = \begin{pmatrix} l & m & n & o & o & p & m & q & r & s & s & t & n & r & u & v & v & w & o & s & v & x & x & y & o & s & v & x & x & y & p & t & w & y & y & z \\ q & m & s & t & r & s & m & l & o & p & n & o & s & o & x & y & v & x & t & p & y & z & w & y & r & n & v & w & u & v & s & o & x & y & v & x \\ u & v & n & r & w & v & v & x & o & s & y & x & n & o & l & m & p & o & r & s & m & q & t & s & w & y & p & t & z & y & v & x & o & s & y & x \\ x & y & s & o & x & v & y & z & t & p & y & w & s & t & q & m & s & r & o & p & m & l & o & n & x & y & s & o & x & v & v & w & r & n & v & u \\ x & v & y & x & o & s & v & u & w & v & n & r & y & w & z & y & p & t & x & v & y & x & o & s & o & n & p & o & l & m & s & r & t & s & m & q \\ z & y & y & w & t & p & y & x & x & v & s & o & y & x & x & v & s & o & w & v & v & u & r & n & t & s & s & r & q & m & p & o & o & n & m & l \end{pmatrix}. \tag{15}$$

Therefore, it is straightforward to see that

$$\bar{M}_1 = \bar{B}_1\bar{B}_1^T, \tag{16}$$

where the superscript T indicates the transpose matrix.

It turns out that, given the large number of distinct matrix elements of B_g, it is no longer possible to explicitly write analytic expressions relating the elements of M_g to those of M_{g-1}. Nevertheless, it is possible to write the exact recurrence relations for the matrix elements of B_g in terms of those of B_{g-1}, from which one can compute the elements of M_g together with the complete eigenvalue spectrum. This finally leads to the free energy and all derived thermodynamical functions for any generation g, as well as to the correlation length

$$\xi_g = \frac{2^g}{\ln(\Lambda_g/\zeta_g)}. \tag{17}$$

In this expression the numerator corresponds to the shortest path connecting the root sites in the gth generation, and ζ_g indicates the second largest eigenvalue (or the third, in case the two largest eigenvalues are degenerate) of M_g. In the Supplemental Material [42] we indicate the expressions of the eigenvalues of $\bar{M}_g$ in terms of its matrix elements.

To account for the effect of the external fields acting only on the internal sites we define the matrix B_1 with matrix elements $(B_1)_{i,jk} = (\bar{B}_1)_{i,jk}\tilde{B}_{jk}$, where

$$\tilde{B}_{jk} = \exp\left[\frac{1}{2k_BT}\sum_{\alpha,\beta=x,y,z}\Big(h_x\big[\Omega_j^{\alpha\beta}\delta(\alpha,x)\delta(\beta,x) + \Omega_k^{\alpha\beta}\delta(\alpha,x)\delta(\beta,x)\big] + h_y\big[\Omega_j^{\alpha\beta}\delta(\alpha,y)\delta(\beta,y) + \Omega_k^{\alpha\beta}\delta(\alpha,y)\delta(\beta,y)\big]\Big)\right]. \tag{18}$$

As in Eq. (16), the matrix M_1 is obtained from

$$M_1 = B_1 B_1^T. \tag{19}$$

The presence of external fields largely increases the number of distinct matrix elements of M_g and B_g. In the Supplemental Material [42] we indicate the general structure of these matrices M_g, as well as the recurrence maps for the matrix elements of M_{g+1} in terms of those of M_g.

B. Real-space RG for the MSZ6 model on DHLs

The idea of a renormalization-group treatment of a statistical model is to rescale lengths by iteratively eliminating degrees of freedom, and renormalizing couplings while looking for scale-invariant conditions associated with the existence of critical phenomena. On a hierarchical lattice, self-similarity prevents the generation of effective couplings involving distant neighbors and increasingly larger sets of lattice sites as real-space degrees of freedom are decimated. Thus, contrary to what generally happens in Bravais lattices of dimension larger than 1, exact real-space renormalization-group solutions of statistical models can be obtained for hierarchical lattices [35,48].

The Hamiltonian $\mathcal{H}_0$ in Eq. (1) is a special case of a more general $\mathcal{H}_{\rm SVD}$ Hamiltonian, which is given by

$$-\frac{\mathcal{H}_{\rm SVD}}{k_B T} = \sum_{(i,j)} \mathcal{U}_{i,j}, \tag{20}$$

in which the sum runs over all nearest-neighbor pairs of sites i and j,

$$\begin{aligned}\mathcal{U}_{i,j} = {} & K\mathbf{q}_i : \mathbf{q}_j + L(\mathbf{q}_i : \mathbf{b}_j + \mathbf{b}_i : \mathbf{q}_j) \\ & + L_2(\mathbf{q}_i : \mathbf{b}_j)(\mathbf{b}_i : \mathbf{q}_j) + M\mathbf{b}_i : \mathbf{b}_j,\end{aligned} \tag{21}$$

and the colon in $\mathbf{q}_i : \mathbf{b}_j$ represents the tensor operation

$$\mathbf{q}_i : \mathbf{b}_j = \sum_{\mu,\nu\in\{x,y,z\}} q_i^{\mu,\nu} b_j^{\mu,\nu}. \tag{22}$$

The two traceless tensors $\mathbf{q}$ and $\mathbf{b}$ (not to be confused with the scalar b representing the number of internal links of the DHL generator) are defined in terms of mutually orthogonal unit vectors $\hat{n}_1$, $\hat{n}_2$, and $\hat{n}_3$, pointing along the principal axes of each nematogen. Therefore,

$$\mathbf{q} = \hat{n}_1 \otimes \hat{n}_1 - \frac{1}{3}\mathbf{I} \quad \text{and} \quad \mathbf{b} = \hat{n}_2 \otimes \hat{n}_2 - \hat{n}_3 \otimes \hat{n}_3, \tag{23}$$

where $\mathbf{I}$ is the 3×3 identity matrix and $\otimes$ the usual outer product. This two-tensor formalism, with $L_2 = 0$, was introduced [33] as a tensor representation of the classical Straley interaction potential between nematogenic units [49], and corresponds to the most general bilinear orientational interaction between biaxial nematogens. The reason for introducing the term proportional to L_2 will become clear below.

The Zwanzig choice consists in restricting the unit vectors $\hat{n}_1$, $\hat{n}_2$, and $\hat{n}_3$ to point along the Cartesian axes, thereby defining six possible nematogen states represented by distinct pairs of tensors $(\mathbf{q}, \mathbf{b})$. The correspondence between $\mathcal{H}_0$ in Eq. (1) and $\mathcal{H}_{\rm SVD}$ in Eq. (20) is obtained if we choose

$$K = \frac{\epsilon}{k_B T}, \quad L = \frac{\Delta}{3}K, \quad L_2 = 0, \quad M = \frac{L^2}{K}. \tag{24}$$

As applied to the DHL shown in Fig. 1, the RSRG scheme amounts to reversing the inflation process, iteratively replacing each instance of the generator by a single link via a summation over the corresponding internal spins. This allows to write the partition function Z_N for a lattice containing N sites,

$$Z_N = \sum_{\{(\mathbf{q},\mathbf{b})\}} \exp\left(-\frac{\mathcal{H}_{\rm SVD}}{k_B T}\right), \tag{25}$$

in terms of the partition function $Z'_{N'}$ for a lattice containing N' sites, with $N/N' = N_g/N_{g-1} \to bp$ as $N \to \infty$ and a renormalized Hamiltonian $\mathcal{H}'_{\rm SVD}$. We explicitly have

$$Z_N = A^{L'} Z'_{N'}, \tag{26}$$

in which L' is the number of links in the renormalized lattice. The parameter A and the effective parameters of $\mathcal{H}'_{\rm SVD}$ are obtained by the summation over the internal sites of a generator. As an example, for $b = 2$, this summation leads to

$$A\, \exp\left(\mathcal{U}'_{i,j}\right) = \sum_k \sum_{\{(\mathbf{q}_k,\mathbf{b}_k)\}} \exp\left(\mathcal{U}_{i,k} + \mathcal{U}_{k,j}\right), \tag{27}$$

with the index k running over the p internal sites of the generator whose end sites are labeled by i and j, and

$$\begin{aligned}\mathcal{U}'_{i,j} = {} & K'\mathbf{q}_i : \mathbf{q}_j + L'(\mathbf{q}_i : \mathbf{b}_j + \mathbf{b}_i : \mathbf{q}_j) \\ & + L'_2(\mathbf{q}_i : \mathbf{b}_j)(\mathbf{b}_i : \mathbf{q}_j) + M'\mathbf{b}_i : \mathbf{b}_j.\end{aligned} \tag{28}$$

Evaluating Eq. (27) for the possible choices of $(\mathbf{q}_i, \mathbf{b}_i)$ and $(\mathbf{q}_j, \mathbf{b}_j)$ leads to five independent relations between the couplings

$$\{x_1, x_2, x_3, x_4\} \equiv \{\tanh K, \tanh L, \tanh L_2, \tanh M\},$$

and the renormalized couplings

$$\{x'_1, x'_2, x'_3, x'_4\} \equiv \{\tanh K', \tanh L', \tanh L'_2, \tanh M'\},$$

plus the parameter A. See the Appendix for explicit results for $b = 2$. Note that it is convenient to use the hyperbolic tangent to deal with cases in which one or more of the parameters K, L, L_2, and M diverge. Eliminating A from these relations yields expressions for the couplings $\{x'_i\}$ in terms of $\{x_i\}$ which can be written in the form

$$x'_i = f_i(x_1, x_2, x_3, x_4) \tag{29}$$

for $i \in \{1, 2, 3, 4\}$. These recursion relations define the renormalization-group (RG) transformation of the model. We note that omitting the term proportional to L_2 in Eq. (21) would render this system of equations indeterminate, as the five independent relations between $\{A\} \cup \{x'_i\}$ and $\{x_i\}$ would be reduced to only 3. We remark that the term proportional to L_2 is nonlinear but respects the expected symmetries of a nematic phase.

Inspection of the functions f_i shows that the choice in Eq. (24) is not invariant under the recursion relations in Eq. (29). Thus, the form of the Hamiltonian in Eq. (1) is not preserved by the RG transformation, in contrast with the form of the Hamiltonian in Eq. (20).

We now restrict the investigation to the initial points in the parameter space which are compatible with the geometric-mean condition and the range $0 \leqslant \Delta \leqslant 3$, and thus with

Eq. (24). The accessible fixed points $\{x_i^*\}$ of the RG transformation are given by the solutions of

$$x_i^* = f_i(x_1^*, x_2^*, x_3^*, x_4^*). \tag{30}$$

We may start with the trivial coordinates

$$\{x_i^*\}_I = \{0, 0, 0, 0\}, \tag{31}$$

which are associated with an isotropic phase. Also, we may start with

$$\{x_i^*\}_{U_+} = \{1, 0, 0, 0\}, \tag{32}$$

which are associated with a rodlike uniaxial phase

$$\{x_i^*\}_{U_-} = \{1, 1, 1, 0\}, \tag{33}$$

associated with a disklike uniaxial phase, and

$$\{x_i^*\}_B = \{1, 1, 1, -1\}, \tag{34}$$

associated with the biaxial phase.

As usual, the critical behavior is related to the unstable fixed points of the RG transformation. The stability analysis is based on the eigenvalues of the matrix R whose elements are defined by

$$R_{i,j} = \left.\frac{\partial f_j}{\partial x_i}\right|_{\{x_i^*\}}. \tag{35}$$

Further details about specific examples, including coordinates of the unstable fixed points, are provided in the next section.

IV. RESULTS AND NUMERICAL ANALYSIS OF THE RG FLUXES

According to the approach described in Sec. III A, the maps for the free energy and its derivatives were iterated numerically until $g = 50$, at the stage in which the solutions converge to fixed values with a relative discrepancy between two successive generations of order 10^{-16}. We considered $\epsilon = k_B = 1$, several values of $\Delta \in [0, 3]$, and iterated the maps as a function of T for the range necessary to cover both transitions, with temperature increment of 10^{-2}. In Fig. 2, we draw the specific heat $c = -T\frac{\partial^2 f}{\partial T^2}$ as a function of T for $\Delta = 0,\ 0.8,\ 1$, and 1.6.

For $\Delta \notin \{0, 1, 3\}$ two cusps are observed at temperatures $T_{\rm BU}$ and $T_{\rm UI}$, the critical temperatures for the biaxial-uniaxial and uniaxial-isotropic phase transitions, respectively. The value $c_{\rm BU}$ of the specific heat at $T_{\rm BU}$ is always smaller than the corresponding value at $T_{\rm UI}$. However, the values of c at all cusps are always smaller than $c_{{\rm UI},\Delta=0}$, the height of the single cusp at $T_{{\rm UI},\Delta=0}$ for $\Delta = 0$, when the biaxial phase is not observed for any $T > 0$. An exception to this scenario occurs at $\Delta = 3.0$, in which case there is only one cusp with the same value $c_{{\rm UI},\Delta=0}$ at a much higher temperature $T_{\rm UI}$. This behavior for $\Delta = 3$ can be understood by the fact that all the energy levels at $\Delta = 3$ are twice as large as those obtained at $\Delta = 0$. When Δ increases in the interval $\Delta \in (0, 1)$, the values of $T_{\rm BU}$ and $T_{\rm UI}$ approach each other and coalesce at a temperature T_L that characterizes a Landau multicritical point, at $\Delta = 1$. At this special point, the $c \times T$ curve is smooth, with no hint of a singular critical behavior. However, for other thermodynamic functions a critical behavior appears in the context of a biaxial-isotropic (BI) transition. Some specificities related to the critical behavior at $\Delta = 1$ will be discussed later on. When Δ further increases in the interval $\Delta \in (1, 3)$ the values of $T_{\rm BU}$ and $T_{\rm UI}$ move apart.

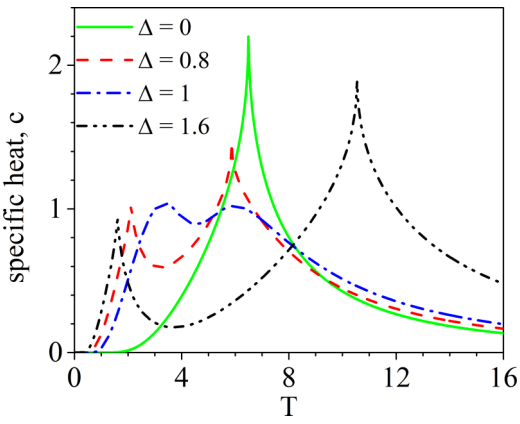

FIG. 2. Specific heat as a function of temperature for $\Delta = 0$ [light gray (green) solid line], 0.8 [gray (red) dashes], 1 [dark gray (blue) dashed-dotted], 1.6 (black dashed-dotted-dotted). For $\Delta = 0$ only one peak is observed, whereas for $\Delta = 0.8$ and 1.6 two peaks are observed. The lower peak is always at a lower temperature than the one for $\Delta = 0$. At the multicritical Landau point ($\Delta = 1$), the curve looks smooth curve for all values of T.

In Fig. 3, we show curves of $\xi \times T$ for four different values of $\Delta = 0,\ 0.8,\ 1$, and 1.6. For the sake of a better understanding, we find it useful to use subscripts BU, UI, and BI to describe each of the three distinct phase transitions. When one works within the TM approach, the correlation length is defined in terms of the largest eigenvalue Λ of M and the second largest eigenvalue distinct from Λ. Let us denote the three largest eigenvalues of the TM, in decreasing order, by Λ, ζ, and Θ. For the MSZ model on DHL we have found that Λ and ζ coalesce for all $T \leqslant T_{\rm UI}$. Thus, while we define $\xi_{\rm UI}$ in terms of Λ and ζ for $T > T_{\rm UI}$, we have found that the BU transition at $T_{\rm BU} < T_{\rm UI}$ can be characterized by $\xi_{\rm BU}$, which is defined in terms of Λ and Θ. At $\Delta = 1$, the BI transition is also investigated by $\xi_{\rm BI}$ defined in terms of Λ and ζ for $T > T_{\rm BI}$.

In Fig. 3(a), we illustrate the typical behavior of $\xi_{\rm UI}$. For $\Delta = 0$, this correlation length diverges at $T_{\rm UI} = 6.4921\ldots$, the same temperature at which the specific heat cusp occurs. As Λ and ζ coalesce within a precision $\sim 10^{-16}$ for $T < T_{\rm UI}$, $\xi_{\rm UI}$ is characterized by a numerical divergence in that temperature interval. The behavior of $\xi_{\rm UI}$ for $T > T_{\rm UI}$ is typical of a second-order phase transition, from which it is possible to evaluate the critical exponent ν. The scenario for $\Delta = 0.8$ shown in Fig. 3(b) indicates a similar divergence of $\xi_{\rm UI}$, while there are two divergences of $\xi_{\rm BU}$ at both $T_{\rm BU} = 2.1173\ldots$ and $T_{\rm UI} = 5.8702\ldots$, whereby the coalescence between Λ and Θ is observed only for $T < T_{\rm BU}$. Thus, for $0 < \Delta < 3,\ \Delta \neq 1$, two continuous phase transitions are observed. The fact that the uniaxial-isotropic transition is predicted to be continuous is in contrast with the (weak) first-order transitions predicted by the experimental results. On the other hand, mean-field treatments generally predict a much stronger first-order uniaxial-isotropic transition [1].

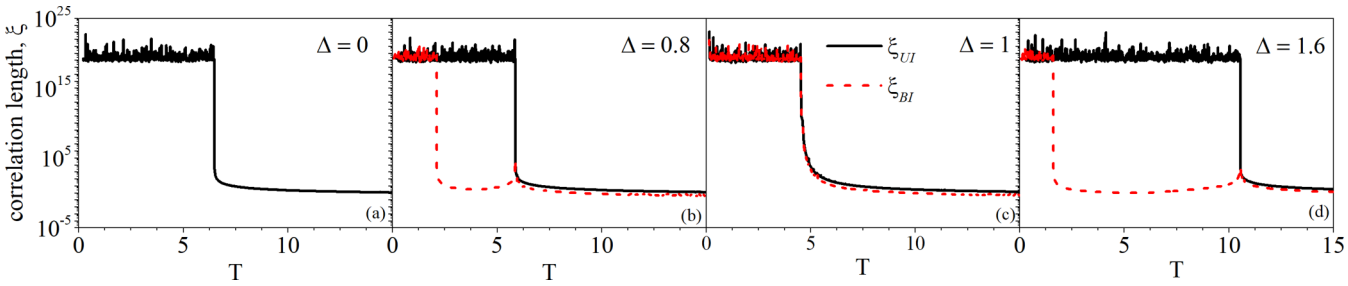

FIG. 3. Correlation length $\xi_{\rm UI}$ (black solid line) and $\xi_{\rm BI}$ [gray (red) dashes] as a function of temperature for $\Delta = 0$ (a), $\Delta = 0.8$ (b), $\Delta = 1$ (c), and $\Delta = 1.6$ (d).

Finally, regarding Fig. 3(c), we also observe a clear divergence of $\xi_{\rm BI}$ for $\Delta = 1$ at $T_{\rm BI} = 4.582\ldots$, which characterizes the Landau point, where the four phases meet: isotropic, biaxial, and two uniaxial phases, a calamitic (rodlike) phase for $\Delta < 1$ and a discotic (disklike) phase for $\Delta > 1$. The behavior of the correlation length contrasts with the curve $c \times T$ for $\Delta = 1$, shown in Fig. 2, which is completely smooth, even at $T_{\rm BI}$. However, when we consider the limits $\Delta \to 1^{-(+)}$, the observed pattern consists of two smooth Shottky maxima, placed respectively to the left of a small cusp at $T_{\rm BU}$ and to the right of another small cusp at $T_{\rm UI}$. At the Landau point, the two cusps disappear when $T_{\rm BU}$ and $T_{\rm UI}$ coalesce at $T_{\rm BI}$. By way of contrast, the two curves for ξ_B and ξ_U also get closer and closer in the same limit, but each of them preserves its divergent character at $T_{\rm BI}$ for $\Delta = 1$. The reasons for this unexpected behavior will be discussed later in this section, together with the evaluation of the critical exponents.

In Figs. 4 and 5 we illustrate the dependence of m_x, m_y, S, and η with respect to T for several values of Δ that correspond to all different patterns. Our results show that, irrespective of the shapes of the curves for m_x and m_y observed for different values of Δ, S, and η vanish identically for, respectively, $T > T_{\rm UI}$ and $T > T_{\rm BU}$. At the Landau point we also observe a consistent scenario, where m_x and m_y coincide, both vanishing at $T_{\rm BI}$.

The general susceptibilities, which are second derivatives with respect to the field components $\chi_x \equiv (\partial^2 f_g/\partial h_x^2)|_{h_x=0}$ and $\chi_y \equiv (\partial^2 f_g/\partial h_y^2)|_{h_y=0}$, directly reflect the behavior of m_x and m_y shown in Fig. 4. At $\Delta = 0$, there is only one critical divergence at $T_{\rm UI}$ for both field components χ_x and χ_y. For $\Delta > 1$, divergent behaviors are observed at $T_{\rm BU}$ and $T_{\rm UI}$ for both χ_x and χ_y. On the other hand, as the curve for m_x at $T_{\rm BU}$ is smooth when $\Delta < 1$, χ_x is characterized by a single critical behavior at $T_{\rm UI}$ while χ_y diverges at both $T_{\rm BU}$ and $T_{\rm UI}$. The behavior of χ_x and χ_y when $\Delta = 1$ can be also similarly inferred from m_x and m_y. They coincide with each other, diverging at $T_{\rm BI}$. These features are clearly illustrated in Fig. 6.

The uniaxial and biaxial susceptibilities χ_S and χ_η can be obtained by summing or subtracting χ_x and χ_y in accordance with the expressions for S and η in Eqs. (10) and (11). The overall aspects of the dependence of χ_x and χ_y as functions of T are essentially the same as those displayed in Fig. 6

We remark that, from the present results, the divergences of ξ provide the best estimations for the critical temperatures for all values of Δ in the interval $0 \leqslant \Delta \leqslant 3$, with at least 14 digits. They have been used to draw the phase diagram in the (T_c, Δ) plane in Fig. 7, with the regions associated with the four different phases. We observe that the phase diagram shares the same aspect as other theoretical phase diagrams for biaxial liquid crystals [2,28,32,50,51]. The main difference lies in the fact that, as already mentioned, the UI (or nematic-isotropic) transition is experimentally known to be weakly first order. The second-order UI phase transition of the MSZ model in DHL is most probably an artifact of the lattice, as it has been extensively discussed in the case of the q-state Potts model that always exhibits continuous transitions in DHLs. Indeed, as reported in [44], on the basis of an extensive use of RSRG analyses, no first-order phase transitions have been found in these structures. This is in contrast with the Potts model on the square lattice, which is known to display a second-order phase transition for $q \leqslant 4$ and first-order transitions for $q > 4$ [43].

The very precise values of the critical temperatures obtained with the TM method make it possible to independently estimate the critical exponents associated with various thermodynamic functions for all observed transitions. From the numerical calculation of the logarithm of the associated

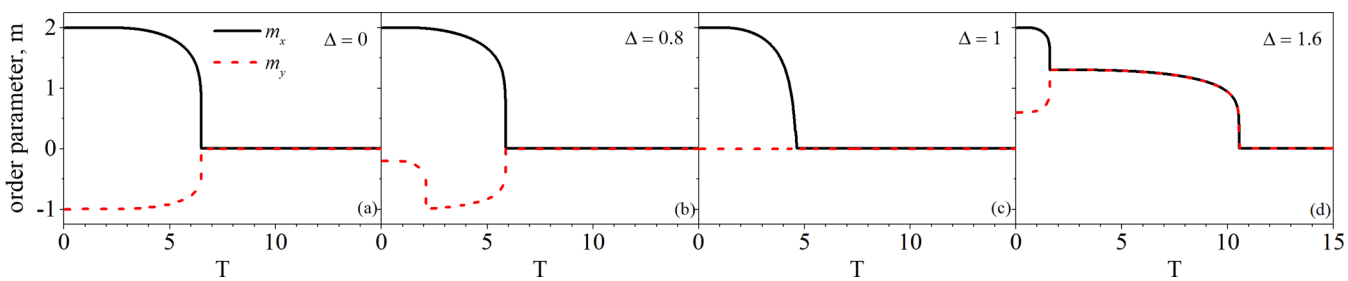

FIG. 4. First derivatives m_x (black solid line) and m_y [gray (red) dashes] of the free energy with respect to the fields h_x and h_y as a function of temperature for $\Delta = 0$ (a), 0.8 (b), 1 (c), and 1.6 (d).

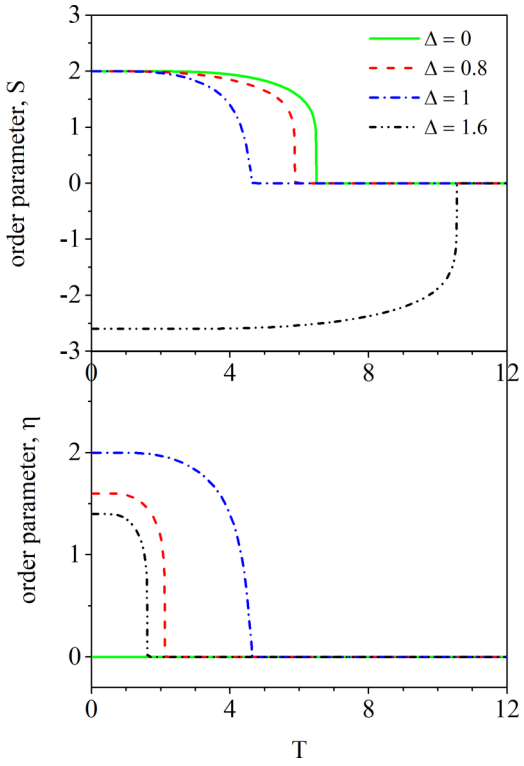

FIG. 5. Uniaxial S and biaxial η order parameters as a function of temperature for several values of Δ. Line types and colors are the same used in Fig. 2.

functions, in terms of reduced temperature $t = |T - T_c|/T_c$, we obtain the asymptotic values

$$c \sim (T - T_c)^{-\alpha}, \quad c \sim (T_c - T)^{-\alpha'}, \tag{36}$$

$$\xi \sim (T - T_c)^{-\nu}, \quad \xi \sim (T_c - T)^{-\nu'}, \tag{37}$$

$$S \sim (T_c - T)^{\beta_S}, \quad \eta \sim (T_c - T)^{\beta_\eta}, \tag{38}$$

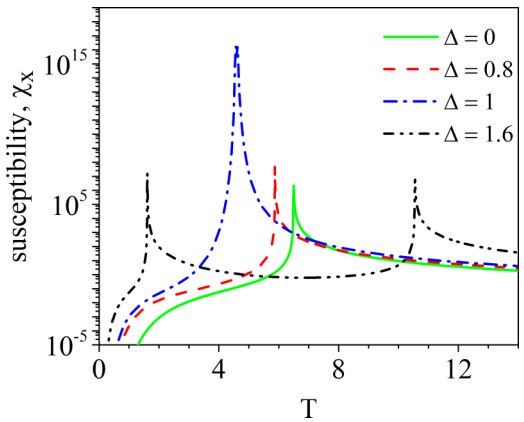

FIG. 6. General susceptibility χ_x as a function of temperature for several values of Δ. The susceptibility χ_y shows quite similar profiles, with exception of the presence of another divergence at the BU transition temperature for $\Delta < 1$. Line types and colors are the same used in Fig. 2.

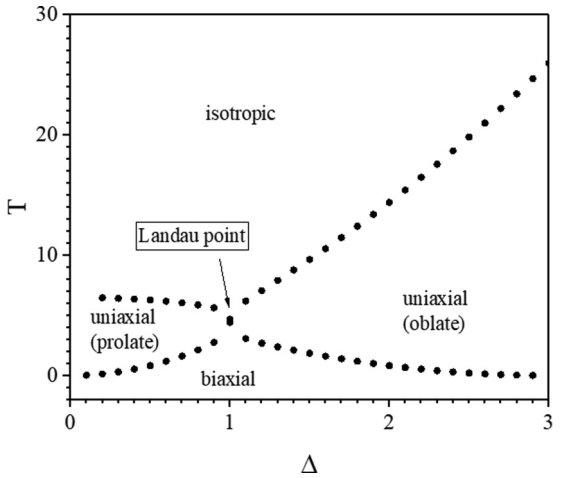

FIG. 7. Phase diagram in the $\Delta \times T$ plane. The Landau point is located at $(\Delta, T) = (1, 4.582)$. Each point in the diagram was obtained by iterating the maps with a fixed value of the biaxiality parameter Δ. All lines represent continuous transitions.

in which T_c may represent $T_{\rm UI}$, $T_{\rm BU}$, and $T_{\rm BI}$. In the Supplemental Material [42] we present some graphs illustrating the used procedure. The values of the slopes in these graphs, which correspond the critical exponents, are shown in Table I for UI, BU, and the $\Delta = 1$ BI transitions. We remark that, for the BI transition, the exponents α and α' could not be independently evaluated within the TM approach, as the specific heat curves appear completely smooth.

The values that we have obtained can be used to test the Rushbrooke, $\alpha' + 2\beta + \gamma' = 2$, and the hyperscaling relations, $\nu d = 2 - \alpha$, in the TM approach. Our estimates indicate that, for the UI and BU transitions, these relations are satisfied within an error of less than 1%. However, for the BI transitions, we tested the accuracy of the TM approach by evaluating the values of α and α' using the above relations. The two obtained values differ by ~6%. The UI and BU transitions are in different universality classes. However, the universality class of the uniaxial-isotropic transition for the intrinsically uniaxial model, for $\Delta = 0$, remains the same with the addition of biaxiality. That is, this transition continues to belong to the same universality class of the three-state Potts model in the DHL, while the BU transition belongs to the same universality class as the Ising model in the same lattice [52,53]. Finally, we were unable to identify whether the BI transition belongs to any previously described universality class.

It is fortunate that our calculations lead to critical behaviors compatible with three-state Potts and Ising models.

TABLE I. Critical exponents. In the biaxial-isotropic transition, α and α' were obtained via hyperscale and Rushbrooke relations.

	ν	α	α'	β	γ'
Uniaxial-isotropic	1.205	−0.418	−0.41	0.159	2.091
Biaxial-uniaxial	1.338	−0.68	−0.678	0.1617	2.3531
Biaxial-isotropic	5.99	−9.98	−9.38	0.49	10.4

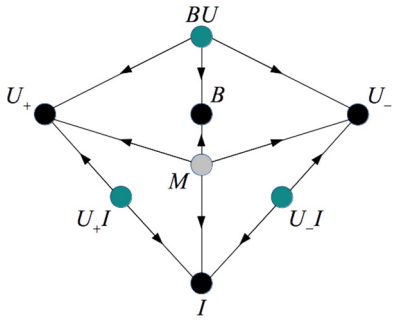

FIG. 8. Sketch showing a subset of the flows of the RG transformation. Labels are defined in the main text.

In the transition between the uniaxial nematic and isotropic structures, the Hamiltonian terms associated with biaxiality are irrelevant, as it can be checked by looking at the eigenvectors of the renormalization-group relations in the vicinity of the appropriate fixed points, indicated in Eqs. (39) and (40) below. On the other hand, uniaxial order, in our MSZ6 model, involves the breaking of a threefold symmetry, hence, the transition between the uniaxial and the isotropic phases must be in the three-state Potts universality class. In addition, slightly above the critical temperature of the transition between uniaxial and biaxial phases, there is already a partial symmetry breaking associated with uniaxial order. As such order is threefold degenerate, out of the sixfold degeneracy of the Hamiltonian there remain two compatible states only, so that breaking the remaining symmetry involves a transition in the Ising universality class. Of course, the observation of these universality classes is an artifact of the discretization leading to the MSZ6 model, and is not expected to be reproduced for rotationally continuous models.

In the case of the "thermal" exponents α and ν, a check is provided by the RSRG treatment of Sec. III B, which we then use to treat the $b = p = 2$ with the transfer-matrix method. The fixed points associated with the various phases are listed in Sec. III B. We now discuss the unstable fixed points associated with the transitions between those phases, which can be obtained numerically from the solutions of Eq. (30), with values of up to 4 digits.

There are two fixed points related to the UI transition,

$$\{x_i^*\}_{\mathrm{U_+I}} = \{0.8824, 0, 0, 0\}, \tag{39}$$

which governs the transition between the isotropic and the rodlike uniaxial phases, and

$$\{x_i^*\}_{\mathrm{U\_I}} = \{0.3333, 0.3333, 0, 0.3333\}, \tag{40}$$

which governs the transition between the isotropic and the disklike uniaxial phases. On the other hand, there is a single fixed point governing the BU transition

$$\{x_i^*\}_{\mathrm{BU}} = \{1, 0.9815, -0.7231, 0.2956\}. \tag{41}$$

Finally, there is a multicritical fixed point associated with the maximum-biaxiality case $\Delta = 1$:

$$\{x_i^*\}_{M} = \{0.9872, 0.7900, -0.1869, 0.1869\}. \tag{42}$$

A simplified scheme showing part of the flows between the various fixed points is presented in Fig. 8.

The critical exponents can be calculated from the behavior of the RG equations around a given critical fixed point $\{x_i^*\}$. If we are sufficiently close to this fixed point, we write

$$|x' - x^*\rangle = R\,|x - x^*\rangle, \tag{43}$$

in which R is the matrix defined in Eq. (35), and $|\ldots\rangle$ is the vector whose components are given by $x_i - x_i^*$. If we denote by λ_j an eigenvalue of the matrix R and by $|v_j\rangle$ and $\langle v_j|$ the corresponding normalized right and left eigenvectors, so that we have the scalar products $\langle v_l|v_j\rangle = \delta_{jl}$, we can write

$$|x' - x^*\rangle = \sum_{j=1}^{4} u_j\,|v_j\rangle \tag{44}$$

in which the scaling fields u_j are given by

$$u_j = \langle v_j|x - x^*\rangle. \tag{45}$$

If we order the eigenvalues of R so that $|\lambda_1| \geqslant |\lambda_2| \geqslant |\lambda_3| \geqslant |\lambda_4|$, it is clear from iterating Eq. (43) that the RG flow near the fixed point is governed by λ_1, as long as the corresponding scaling field u_1 is not negligible.

The RG eigenvalues y_j around a critical fixed point are related to the eigenvalues λ_j of the matrix R given by Eq. (35) so that

$$y_j = \frac{\ln \lambda_j}{\ln b}. \tag{46}$$

In particular, if λ_t is the largest eigenvalue of R with a nonvanishing scaling field, the correlation-length critical exponent ν is related to the corresponding "thermal" RG eigenvalue y_t:

$$\nu = \frac{1}{y_t} = \frac{\ln b}{\ln \lambda_t}. \tag{47}$$

Around $\{x_i^*\}_{\mathrm{UI}}$ we obtain $y_t = y_1 \simeq 1.778$, so that

$$\nu_{\mathrm{UI}} \simeq 1.205, \tag{48}$$

in excellent agreement with the numerical estimate from the TM calculations. It should be pointed out that K is the only nonzero parameter at $\{x_i^*\}_{\mathrm{UI}}$, and that the uniaxial order parameter S becomes nonzero at the UI transition. Thus, we should expect that, starting from a temperature below T_{UI}, under the RG transformation the parameter K flows towards $K \to \infty$ (which means $x_1 \to 1$), as we have indeed checked.

For the biaxial-uniaxial transition, we obtain $y_t = y_1 \simeq 1.679$, which leads to the correlation-length exponent

$$\nu_{\mathrm{BU}} \simeq 1.338, \tag{49}$$

which is again in excellent agreement with TM results.

Finally, for $\Delta = 1$ there is a single biaxial-isotropic transition governed by the fixed point $\{x_i^*\}_M$. The associated thermal RG eigenvalue is $y_t = y_2 \simeq 1.123$ rather than $y_1 \simeq 1.790$, since the scaling field u_1 becomes negligible as the fixed point is approached starting from the geometric-mean condition in the neighborhood of the Landau temperature $T_c \simeq 4.581\ldots$. This is compatible with the fact that the direction defined by the eigenvector associated with the largest eigenvalue of R at $\{x_i^*\}_M$ leads to flows towards the uniaxial phases, which are not expected to be realized starting from the maximally biaxial case $\Delta = 1$. The correlation-length critical exponent is

$$\nu_{\mathrm{BI}} \simeq 5.993, \tag{50}$$

which is again in agreement with the transfer-matrix results. We remark that, for this particular value of ν, the hyperscale relation indicates that $\alpha \simeq -9.986$, which agrees quite well with the value in Table I, and explains why the specific heat curve looks completely smooth around $T_{\rm BI}$.

Of course, it is possible to add formal field terms to $\mathcal{H}_{\rm SVD}$ in order to investigate the "magnetic" scaling fields and determine the order-parameter critical exponents. However, the complete agreement between the obtained results within the TM and RG approaches for α and ν, as well as the independent check obtained by the Rushbrooke relations, provide enough confidence for the values of β and γ obtained by the TM approach.

It is worth to compare the critical exponents obtained in this work with the corresponding experimental results for the uniaxial-biaxial transition. Boonbrahm and Saupe [54] and later Melnik *et al.* [55] obtained $\beta = 0.38 \pm 0.03$ and $\gamma = 1.29 \pm 0.08$, for the BU transition in a lyotropic mixture. These values are in reasonable agreement with the exponents for the XY model in three dimensions. However, the critical behavior for the BU transition in this case seems to depend on the relative composition of the mixture and therefore could not be universal [56]. In any case, the values of critical exponents for the BU transition in Table I are quite different from the experimental results. We still do not have experimental data for the BU transition in thermotropic liquid crystals.

V. CONCLUSIONS

We used real-space renormalization-group techniques to analyze global phase transitions and critical phenomena in a class of six-state Maier-Saupe-Zwanzig models, whose mean-field version is known to lead to a sequence of biaxial nematic, uniaxial nematic, and disordered structures, as the temperature increases, and to the possibility of occurrence of a Landau multicritical point. From an exact decimation procedure in a diamond hierarchical lattice, we regain a similar qualitative picture, which is in overall agreement with experimental findings for biaxial nematic systems. Results are confirmed by an alternative renormalization-group calculation on the basis of a transfer-matrix technique. According to these calculations, the biaxial-uniaxial transition belongs to the same universality class of the Ising model on the diamond lattice. The uniaxial-isotropic transition, however, belongs to the universality class of the Potts model on the diamond hierarchical lattice, which is also the same universality class of the much simpler three-state uniaxial MSZ lattice model. We point out that the weak uniaxial-disordered transition of our calculations is far from the weak first-order transition, as it is found in mean-field calculations, and it is generally accepted in the literature. This type of behavior may be attributed to special features of the hierarchical lattices. Along the same lines of this work, it is certainly possible to carry out additional investigations, using more elaborate hierarchical lattices and other generators of the renormalization group.

ACKNOWLEDGMENTS

This work was supported by the Brazilian agency CNPq through Grants No. 422561/2018-5 and No. 304257/2019-2 (R.F.S.A.). R.F.S.A. acknowledges the support of the National Institute of Science and Technology for Complex Systems (INCT-SC Brazil). A. P. Vieira and S. R. Salinas acknowledge financial support from INCT/FCx, NAP/FCx, and CNPq.

APPENDIX: DETAILS OF THE RSRG CALCULATION

The explicit forms of the relations obtained from Eq. (27) in the case $b = 2$ are

$$Ae^{\frac{2}{3}K'+2M'} = \left(e^{\frac{4}{3}K+4M} + e^{\frac{4}{3}K-4M} + e^{-\frac{2}{3}K+4L+2M+2L_2} + 2e^{-\frac{2}{3}K-2M-2L_2} + e^{-\frac{2}{3}K-4L+2M+2L_2}\right)^p, \tag{A1}$$

$$Ae^{\frac{2}{3}K'-2M'} = \left(2e^{\frac{4}{3}K} + 2e^{-\frac{2}{3}K+2L} + 2e^{-\frac{2}{3}K-2L}\right)^p, \tag{A2}$$

$$Ae^{-\frac{1}{3}K'+2L'+M'+L_2'} = \left(2e^{\frac{1}{3}K+3M+2L+L_2} + 2e^{\frac{1}{3}K-3M-L_2} + 2e^{-\frac{2}{3}K-2L}\right)^p, \tag{A3}$$

$$Ae^{-\frac{1}{3}K'-2L'+M'+L_2'} = \left(2e^{\frac{1}{3}K+3M-2L+L_2} + 2e^{\frac{1}{3}K-3M-L_2} + 2e^{-\frac{2}{3}K+2L}\right)^p, \tag{A4}$$

$$Ae^{-\frac{1}{3}K'-M'-L_2'} = \left(2e^{\frac{1}{3}K+M-L_2} + e^{\frac{1}{3}K-M-2L+L_2} + e^{\frac{1}{3}K+2L-M+L_2} + e^{-\frac{2}{3}K-2M-2L_2} + e^{-\frac{2}{3}K+2M+2L_2}\right)^p, \tag{A5}$$

from which expressions of the form shown in Eq. (29) follow by isolating K', L', L_2', and M' in terms of K, L, L_2, and M. Although straightforward, this procedure yields rather long expressions which we refrain from presenting here.

[1] P. G. de Gennes and J. Prost, *The Physics of Liquid Crystals, 2nd edition* (Clarendon, Oxford, 1993).
[2] S. Singh, Phys. Rep. **324**, 107 (2000).
[3] E. J. Davis and J. W. Goodby, Classification of liquid crystals according to symmetry, in *Handbook of Liquid Crystals* (American Cancer Society, Atlanta, 2014), Chap. 2, pp. 1–32.
[4] M. J. Freiser, Phys. Rev. Lett. **24**, 1041 (1970).
[5] L. J. Yu and A. Saupe, Phys. Rev. Lett. **45**, 1000 (1980).
[6] F. Yang and J. R. Sambles, Physical investigations of biaxial nematic liquid crystals, in *Handbook of Liquid Crystals* (American Cancer Society, Atlanta, 2014), Chap. 13, pp. 1–34.

[7] E. Mirzad Rafael, D. Corbett, A. Cuetos, and A. Patti, Soft Matter **16**, 5565 (2020).

[8] G. Luckhurst, Thin Solid Films **393**, 40 (2001), Proceedings from the 4th International Conference on Nano-Molecular Electronics.

[9] B. R. Acharya, A. Primak, and S. Kumar, Phys. Rev. Lett. **92**, 145506 (2004).

[10] L. A. Madsen, T. J. Dingemans, M. Nakata, and E. T. Samulski, Phys. Rev. Lett. **92**, 145505 (2004).

[11] G. R. Luckhurst, Nature (London) **430**, 413 (2004).

[12] E. van den Pol, A. V. Petukhov, D. M. E. Thies-Weesie, D. V. Byelov, and G. J. Vroege, Phys. Rev. Lett. **103**, 258301 (2009).

[13] G. R. Luckhurst and T. J. Sluckin, *Biaxial Nematic Liquid Crystals* (Wiley, Hoboken, NJ, 2015).

[14] W. Maier and A. Saupe, Z. Naturforsch. A **15**, 287 (1960).

[15] R. Zwanzig, J. Chem. Phys. **39**, 1714 (1963).

[16] C. Shih and R. Alben, J. Chem. Phys. **57**, 3055 (1972).

[17] Z. Chen and J. M. Deutch, J. Chem. Phys. **80**, 2151 (1984).

[18] M. J. de Oliveira and A. M. Figueiredo Neto, Phys. Rev. A **34**, 3481 (1986).

[19] M. P. Taylor and J. Herzfeld, Phys. Rev. A **44**, 3742 (1991).

[20] E. F. Henriques and V. B. Henriques, J. Chem. Phys. **107**, 8036 (1997).

[21] S. Belli, A. Patti, M. Dijkstra, and R. van Roij, Phys. Rev. Lett. **107**, 148303 (2011).

[22] A. B. G. M. Leferink op Reinink, S. Belli, R. van Roij, M. Dijkstra, A. V. Petukhov, and G. J. Vroege, Soft Matter **10**, 446 (2014).

[23] R. A. Sauerwein and M. J. de Oliveira, J. Chem. Phys. **144**, 194904 (2016).

[24] J. P. Straley, J. Chem. Phys. **57**, 3694 (1972).

[25] A. Cuetos, M. Dennison, A. Masters, and A. Patti, Soft Matter **13**, 4720 (2017).

[26] A. Patti and A. Cuetos, Mol. Simul. **44**, 516 (2018).

[27] E. do Carmo, D. B. Liarte, and S. R. Salinas, Phys. Rev. E **81**, 062701 (2010).

[28] E. S. Nascimento, E. F. Henriques, A. P. Vieira, and S. R. Salinas, Phys. Rev. E **92**, 062503 (2015).

[29] E. S. Nascimento, A. P. Vieira, and S. R. Salinas, Braz. J. Phys. **46**, 664 (2016).

[30] S. R. Salinas and E. S. Nascimento, Mol. Cryst. Liq. Cryst. **657**, 27 (2017).

[31] A. Petri and S. R. Salinas, Liq. Cryst. **45**, 980 (2018).

[32] N. Boccara, R. Mejdani, and L. De Seze, J. Phys. (Paris) **38**, 149 (1977).

[33] A. M. Sonnet, E. G. Virga, and G. E. Durand, Phys. Rev. E **67**, 061701 (2003).

[34] E. do Carmo, A. P. Vieira, and S. R. Salinas, Phys. Rev. E **83**, 011701 (2011).

[35] R. B. Griffiths and M. Kaufman, Phys. Rev. B **26**, 5022 (1982).

[36] Z. R. Yang, Phys. Rev. B **38**, 728 (1988).

[37] Z.-Z. Zhang, S.-G. Zhou, and T. Zou, Eur. Phys. J. B **56**, 259 (2007).

[38] B. Hu, Phys. Rev. Lett. **55**, 2316 (1985).

[39] J.-X. Le and Z. R. Yang, Phys. Rev. E **68**, 066105 (2003).

[40] R. F. S. Andrade and S. T. R. Pinho, Eur. Phys. J. B **34**, 343 (2003).

[41] P. Shukla and T. J. Sluckin, J. Phys. A: Math. Gen. **18**, 93 (1985).

[42] See Supplemental Material at http://link.aps.org/supplemental/10.1103/PhysRevE.103.032111 for analytical expressions of the eigenvalues of the field-free matrix M_g, the general structure of the matrix M_g and the recurrence maps of its elements, the general recurrence maps for the free energy, and an illustration how the critical exponents are evaluated within the TM method.

[43] F. Y. Wu, Rev. Mod. Phys. **54**, 235 (1982).

[44] C. Tsallis and A. C. N. de Magalhães, Phys. Rep. **268**, 305 (1996).

[45] R. F. S. Andrade, Phys. Rev. E **59**, 150 (1999).

[46] R. F. S. Andrade, E. Nogueira, and S. Coutinho, Phys. Rev. B **68**, 104523 (2003).

[47] D. O. C. Santos, E. Nogueira, and R. F. S. Andrade, Phys. Rev. B **73**, 174202 (2006).

[48] M. Kaufman and R. B. Griffiths, Phys. Rev. B **30**, 244 (1984).

[49] J. P. Straley, Phys. Rev. A **10**, 1881 (1974).

[50] F. Biscarini, C. Chiccoli, P. Pasini, F. Semeria, and C. Zannoni, Phys. Rev. Lett. **75**, 1803 (1995).

[51] D. Allender and L. Longa, Phys. Rev. E **78**, 011704 (2008).

[52] W. A. M. Morgado, S. Coutinho, and E. M. F. Curado, J. Stat. Phys. **61**, 913 (1990).

[53] L. da Silva, E. M. F. Curado, S. Coutinho, and W. A. Martinez Morgado, Phys. Rev. B **53**, 6345 (1996).

[54] P. Boonbrahm and A. Saupe, J. Chem. Phys. **81**, 2076 (1984).

[55] G. Melnik, P. Photinos, and A. Saupe, J. Chem. Phys. **88**, 4046 (1988).

[56] L. T. Thieghi, S. M. Shibli, A. M. Figueiredo Neto, V. P. Dmitriev, and P. Tolédano, Phys. Rev. Lett. **80**, 3093 (1998).